Research article

SURFACE and INTERFACE ANALYSIS

Received: 4 December 2013 Revised: 4 April 2014 Accepted: 16 April 2014 Published online in Wiley Online Library

(wileyonlinelibrary.com) DOI 10.1002/sia.5549

XPS study of the surface properties and Ni particle size determination of Ni-supported catalysts

Ana M. Tarditi,[a] Noelia Barroso,[b] Agustín E. Galetti,[b] Luis A. Arrúa,[b] Laura Cornaglia[a] and María C. Abello[b]*

The surface properties of $Ni/MgAl_2O_4$ catalysts doped with Ce or Pr were analyzed by XPS after treatment in an inert and reductive atmosphere at 400 °C. The Ce-promoted solids presented the Ce^{3+}/Ce^{4+} couple on the surface even after treatment in a reductive atmosphere, H_2(5%)/Ar. The promotion effect of Ce on these solids could be associated with their participation on the carbon deposition-removal mechanism. Pr-doped catalysts showed a very high concentration of Pr^{3+} under a reductive atmosphere and the redox behavior associated with the carbon removal could be partially inhibited or become slower. The size of the Ni^0 particles after both an inert and a reductive atmosphere was estimated by XPS intensity ratio using the model proposed by Davis. The results obtained from the Davis model showed that an important increase occurred in Ni particle size after treatment in H_2(5%)/Ar for the Pr-promoted solids. The metal sintering under reductive atmosphere could be the reason for the higher loss of activity of the Pr-doped solids under reforming conditions. Copyright © 2014 John Wiley & Sons, Ltd.

Keywords: $Ni/MgAl_2O_4$ catalyst; Ce or Pr; XPS; Davis model

Introduction

Among renewable energy sources, hydrogen has attracted much attention as an important energy carrier because of its high-energy efficiency and pollutant-free emissions when it is produced from a renewable source. From an environmental point of view, the ethanol steam reforming reaction is a promising alternative to produce hydrogen taking into account that ethanol can be obtained by fermentation of biomass and has a high hydrogen content.

The ethanol steam reforming reaction could be catalyzed by various noble and transition metals. Among them, the noble-metal (Ru, Rh, Pt, Ir, etc.) based solids are the most active and selective ones for hydrogen production.[1,2] However, the high cost of these metals is the main limitation for their application. On the other hand, Ni-supported catalysts have shown to be active and selective for the reaction,[3] with the advantage of being of low costs and high availability. The main problem related with these catalysts is the high deactivation rate due to both the formation of carbonaceous deposits and the sintering of metallic nanoparticles. Deactivation by carbon deposition can be caused by the blockage of the active site or by filamentous carbon accumulation that causes obstruction of the catalytic bed. For Ni-based catalysts, it has been shown that the Ni particle size has significant effects on the carbon formation mechanism.[4,5] As reported by Bengaard *et al.*,[6] smaller particles are more resistant to carbon deposition; even more, carbon formation is not able to proceed when the particles are below a critical size.[6] It is well known that the support considerably affects the activity, selectivity and the long-term stability of the catalyst. A suitable support has to be resistant to the high temperatures attained during the ethanol steam reforming and also be able to maintain the metallic dispersion as high as possible during reaction. Among several solids, spinel-like oxides (AB_2O_4) such as $MgAl_2O_4$ have been applied as catalytic supports because of their low acidity and sintering resistance.[7,8] On the other hand, previous studies have shown that the addition of Ce[8] or Pr[9] to Ni-based catalysts increases the resistance to the formation of carbonaceous deposits.

Praseodymium and cerium are adjacent in the periodic table, and their oxides have many similar characteristics.[10] Praseodymium has a special position within the rare earth elements because it can form a homologous series of oxides with variable valence states (+3 and +4) and a large number of stoichiometrically defined oxides: Pr_nO_{2n-2}, with $n = 4, 7, 9, 10, 11, 12, \infty$[11] the extreme cases being Pr_2O_3 and PrO_2. As ceria, these oxides have high oxygen ion mobility and, therefore, the ability to acquire or release oxygen; meanwhile, they convert their oxidation states between +3 and +4. However, differences have been reported on Rh/CeO_2 and Rh/PrO_x catalysts concerning the relative amount of H_2 that desorbs at low and high temperatures.[12] In studies about interaction with CO, Borchert *et al.* have also reported that CO is not adsorbed on Pr cations (Pr^{3+} or Pr^{4+}), whereas adsorption occurs on Ce^{4+} at room temperature.[13] Besides, Gallego *et al.*[14] have recently studied the influence of Pr on dry methane-reforming catalysts produced from perovskites. These authors have reported a high resistance to deactivation as a

* *Correspondence to: María C. Abello, INTEQUI, Instituto de Investigaciones en Tecnología Química (UNSL-CONICET), Chacabuco y Pedernera, San Luis 5700, Argentina.*
E-mail: cabello@unsl.edu.ar

a *Instituto de Investigaciones en Catálisis y Petroquímica (FIQ, UNL-CONICET), Santa Fe 3000, Argentina*

b *INTEQUI, Instituto de Investigaciones en Tecnología Química (UNSL-CONICET), San Luis 5700, Argentina*

consequence of the redox chemistry of praseodymium oxides. They have suggested that praseodymium oxides have a high facility to reoxidize and could react with CO_2 during the reforming reaction to form PrO_2 and CO.

The ethanol steam reforming reaction to produce hydrogen over Ni catalysts supported on $MgAl_2O_4$ doped with Ce or Pr has been reported in a previous work.[15] Two nickel sources were used: nickel nitrate (Nt) and nickel acetate (Ac). The catalyst prepared from nickel nitrate and doped with Pr showed the lowest average Ni particle size [determined by X-ray diffraction (XRD)], and it was very active during the first 150 min in reaction. After 350 min, the ethanol conversion markedly decreased, and a significant amount of carbon was formed causing the blocking of the reactor. The catalysts modified by Ce were more selective to H_2 and to CO_2. They presented a higher catalytic stability than those modified by Pr. The Ni(Ac)/$MgAl_2O_4$–CeO_2 catalytic system showed the highest ethanol conversion under the conditions studied but an abundant carbon filament formation. The Ni(Nt)/$MgAl_2O_4$–CeO_2 catalyst was also very active (steady ethanol conversion = 95.8%) with a low amount of carbon (0.4 wt.%) and a low conversion loss (6.6%) under the same conditions. This catalyst showed the best overall catalytic performance under the experimental conditions used in that work. The experimental results indicated that there was not a clear relationship between the nature of the dopant with the carbon content and the degree of deactivation. In this work, these catalysts are characterized by XPS, in order to provide new insights related to the factors that influence the catalytic behavior of the solids. The study of the surface composition and the oxidation state under different treatments were carried out, and the Davis model was applied to estimate the Ni^0 particle size by XPS measurements.

Experimental

Catalyst preparation

Ni catalysts supported on $MgAl_2O_4$ modified with rare earths (Ce or Pr) were prepared. The $MgAl_2O_4$ support (MA) was prepared by the citrate method. Citric acid was added to an aqueous solution that contained the stoichiometric quantities of $Al(NO_3)_3{\cdot}9H_2O$ and $Mg(NO_3)_2{\cdot}6H_2O$. An equivalent of acid per total equivalent of metals was used. The solution was stirred for 10 min and held at boiling temperature for 30 min. Then, the solution was concentrated by evaporation under vacuum in a rotavapor at 75 °C until a viscous liquid was obtained. Finally, dehydration was completed by drying the sample in a vacuum oven at 100 °C for 16 h. The sample was calcined in a 100 mL min^{-1} flow under the following program: at 500 °C in N_2 flow for 2 h and then at 700 °C in air for 4 h to remove the carbonaceous residues from citrate chains.[9]

The MA support modified by the addition of 5 wt.% of rare earth was prepared by wet impregnation using an aqueous solution of $Pr(CH_3COO)_3{\cdot}xH_2O$ (Aldrich, 99.9%) or $Ce(CH_3COO)_3{\cdot}xH_2O$ (Aldrich, 99.9 %). The solvent was evaporated in a rotavapor at 75 °C under vacuum. The samples were dried at 100 °C and calcined in air at 600 °C for 2 h. The modified support was denoted as MAX being X = Pr from Pr or Ce from Ce, respectively.

Four supported catalysts with 8 wt.% Ni were prepared by the wet impregnation technique using an aqueous solution of $Ni(NO_3)_2$ $6H_2O$, (Nt), or $Ni(CH_3COO)_2$ $4H_2O$, (Ac). After impregnation, the samples were dried and heated in a 5% H_2/N_2 flow (200 mL min^{-1}) from room temperature to 600 °C at 10 °C min^{-1}; then, they were kept at 600 °C for 2 h. The fresh catalysts were denoted as Ni(Y)/MAX X: Pr or Ce, being indicative of rare earth, and Y: Ac or Nt, indicative of Ni precursor. Hence, Ni(Nt)/MACe indicates a catalyst with 8 wt.% of Ni prepared from nickel nitrate over the MACe support.

Catalyst characterization

All samples were characterized using different physico-chemical methods.

Chemical composition

Praseodymium, cerium and nickel chemical composition was performed by inductively coupled plasma atomic emission spectroscopy (ICP) by using a sequential ICP spectrometer Baird ICP 2070 (BEDFORD, USA) with a Czerny Turner monochromator (1 m optical path). Alkali fusion with $KHSO_4$ and a subsequent dissolution with HCl solution brought the samples into solution.

BET surface area

Brunauer, Emmett and Teller (BET) surface areas were measured using a Micromeritics Gemini V analyzer by adsorption of nitrogen at −196 °C on 100 mg of sample previously degassed at 250 °C for 16 h under flowing N_2.

X-ray diffraction

Diffraction patterns were obtained with a RIGAKU diffractometer operated at 30 kV and 20 mA using Ni-filtered CuKα radiation ($\lambda = 0.15418$ nm) at a rate of 3° min^{-1} from $2\theta = 20°$ to 80°. The powdered samples were analyzed without a previous treatment after deposition on a quartz sample holder. The identification of crystalline phases was made by matching with the JCPDS files.

Basicity properties

Basicity measurements were determined by CO_2 temperature-programmed desorption, CO_2 temperature-programmed desorption, using a conventional flow system with a thermal conductivity detector ~0.2 g was used in each experiment. All samples were prereduced under a (5%)H_2/N_2 flow at 650 °C for 1 h to simulate the catalyst state under reforming conditions. After cooling down to room temperature, the adsorption step started. This step was carried out in pure CO_2 flow for 45 min. Afterwards, the samples were swept with helium for 30 min, and finally, the desorption step was performed from room temperature to 700 °C at a heating rate of 10 °C min^{-1} and 30 mL min^{-1} of helium flow. Continuous voltages from the detector cell and reactor thermocouple were converted to digital signals, amplified with a data acquisition workstation and stored in a PC. The total integrated area of the CO_2 band was considered as a measurement of total basicity. CO_2 uptake expressed as μmoles CO_2 per g_{cat} and the basic site density expressed as μmoles CO_2 per m^2 were estimated after CO_2 calibration.

Transmission electron microscopy

Transmission electron microscopy (TEM) micrograph images were recorded in a FEI Tecnai T20 equipment operated at 200 kV so that irradiation damage was minimized. Specimens were prepared by standard techniques. The histograms of the particle size distribution were obtained by counting over the micrographs at least 150 particles, and the surface average particle size, d_s, was calculated as $d_s = \sum n_i d_i^3 / \sum n_i d_i^2$, where n_i

is the number of particles and d_i is the characteristic particle diameter. The size measurement was performed with the CAD software using the measurement tool and an adequate scaling factor.

X-ray photoelectron spectroscopy

The XPS measurements were carried out using a multitechnique system (SPECS) equipped with a dual Mg/Al X-ray source and a hemispherical PHOIBOS 150 analyzer operating in the fixed analyzer transmission mode. The spectra were obtained with pass energy of 30 eV; an Mg Kα X-ray source was operated at 150 W and 10 kV. The residual pressure inside the analysis chamber was kept at values below 5×10^{-9} mbar. Al 2p, Ni 3p, Mg 2p, Ni 2p, O 1s, Ce 3d or Pr 3d, and C 1s spectra were recorded for each sample. All binding energies (BEs) were referred to the Al 2p line at 74.5 eV; as a consequence, the BE for the C 1s peak was about 284.7 eV. The data treatment was performed with the Casa XPS program (Casa Software Ltd., UK). The peak areas were determined by integration employing a Shirley-type background. The surface atomic ratio was estimated by area integration after the correction with the corresponding sensitivity factor provided by the manufacturer. The samples treated at 600 °C in a 5% H_2/N_2 flow were transferred to the instrument after being exposed to air. Before the XPS measurements, they were treated inside the pre-chamber as follows:

A. Heating in an inert flow (N_2) at 400 °C for 10 min, and atmospheric pressure.
B. Heating in a reductive flow (H_2 5%/Ar) at 400 °C for 10 min after A, and atmospheric pressure.

The A treatment simulates the catalyst initial surface state before the ethanol steam reforming reaction. When the reaction measurements were carried out in a fixed-bed reactor, the catalysts were heated to the reaction temperature under an inert flow, and then, the H_2O/C_2H_5OH mixture was fed. The B treatment simulates the catalyst surface under reforming (a reductive atmosphere is created under reforming conditions).

The XPS measurements were also used to estimate the average Ni^0 particle size. For this purpose, the Davis method[16] was applied using the intensity ratio of two core levels with different kinetic energies of the dispersed phase. The two core levels used were Ni 2p, with a BE approximately at 852 eV, and Ni 3p, located at about 66 eV. A Ni rod was used as the reference material to perform the particle size determination.

Results and discussion

The solids studied in this paper were previously evaluated in the ethanol steam reforming reaction.[15] It was possible to conclude that the Ce-promoted catalysts were more active, selective and stable than the Pr-promoted ones. However, a clear relation between the precursor (nitrate or acetate) and the dopant (Ce or Pr) with the carbon amount and the deactivation could not be obtained.[15] In order to determine the surface properties and their correlation with the catalytic activity, the solids were analyzed by XPS. Some characteristics of the fresh samples extracted from the previous work are summarized in Table 1. The samples were heated under a reductive atmosphere [H_2(5%)/N_2], and this treatment explains the presence of Ni^0 among the XRD phases.[15] Although a surface re-oxidation could occur after exposure to air, an important fraction of Ni^0 remains in metallic state detectable by XRD. The re-oxidation was verified by temperature-programmed reduction. A peak of H_2 consumption appears at about 290 °C for the Ni(Y)/MACe catalysts and at 323 °C for the Ni(Y)/MAPr samples, as previously reported.[15] These consumptions were attributed to the reduction of Ni^{2+} generated by the surface re-oxidation and also to a contribution by the rare earth reduction. After 400 °C, flat TPR profiles were obtained.[15] This temperature was chosen for the two treatments into the XPS pre-chamber.

The surface chemical state and composition of all the catalysts were studied by XPS. Figure 1 shows the XPS spectra of the Ni $2p_{3/2}$ region for the Ni(Nt)/MACe (Fig. 1a) and Ni(Nt)/MAPr (Fig. 1b) catalysts without treatment and after both treatments in the reaction chamber attached to the spectrometer. The Ni 2p doublet was fitted by setting the separation between Ni $2p_{1/2}$ and Ni $2p_{3/2}$ core level peaks as well as between the corresponding shake-up satellites. The doublet ratio was constrained to the expected theoretical value of 1/2 and the full width at the half maximum (fwhm) was fixed for each Ni species. The samples without treatment present a main peak at about 854.6 eV assigned to Ni $2p_{3/2}$ with a shake-up satellite peak centered at 861.7 eV. These BEs could be related with the presence of Ni^{2+} as NiO on the surface of the catalyst, suggesting surface re-oxidation during sample handling before introduction into the spectrometer (in agreement with TPR results). After the two treatments in the reaction chamber of the spectrometer, three peaks are clearly observed at about 851.8–852.4 eV, 855.0–855.4 eV and 860–861 eV (Fig. 1). These BEs can be assigned to Ni^0, Ni^{2+} and

Table 1. Characteristics of the catalysts reduced at 600 °C in a 5% H_2/N_2 flow

Sample	Chemical composition[a], wt.%		S_{BET} m^2 g^{-1}	XRD phases	Basicity,[c] μmol CO_2 m^{-2}
	Ni	RE[b]			
Ni(Nt)/MACe	8.1	5.9	32	$MgAl_2O_4$; CeO_2; Ni^0	8.6 (274.9)
Ni(Ac)/MACe	7.0	6.5	36	$MgAl_2O_4$; CeO_2; Ni^0	10.2 (365.4)
Ni(Nt)/MAPr	8.6	2.9	30	$MgAl_2O_4$; weak peaks of Pr_yO_x; Ni^0	10.3 (310.3)
Ni(Ac)/MAPr	6.8	2.6	29	$MgAl_2O_4$; weak peaks of Pr_yO_x; Ni^0	6.9 (199.2)
MA	—	—	60	—	—

XRD, X-ray diffraction.
[a]Determined by ICP.
[b]Rare earth (Pr or Ce). Nominal loading: 8.0 wt% Ni and 5.0 wt.% RE.
[c]Values between brackets correspond to the basicity expressed as μmol CO_2 g_{cat}^{-1}.

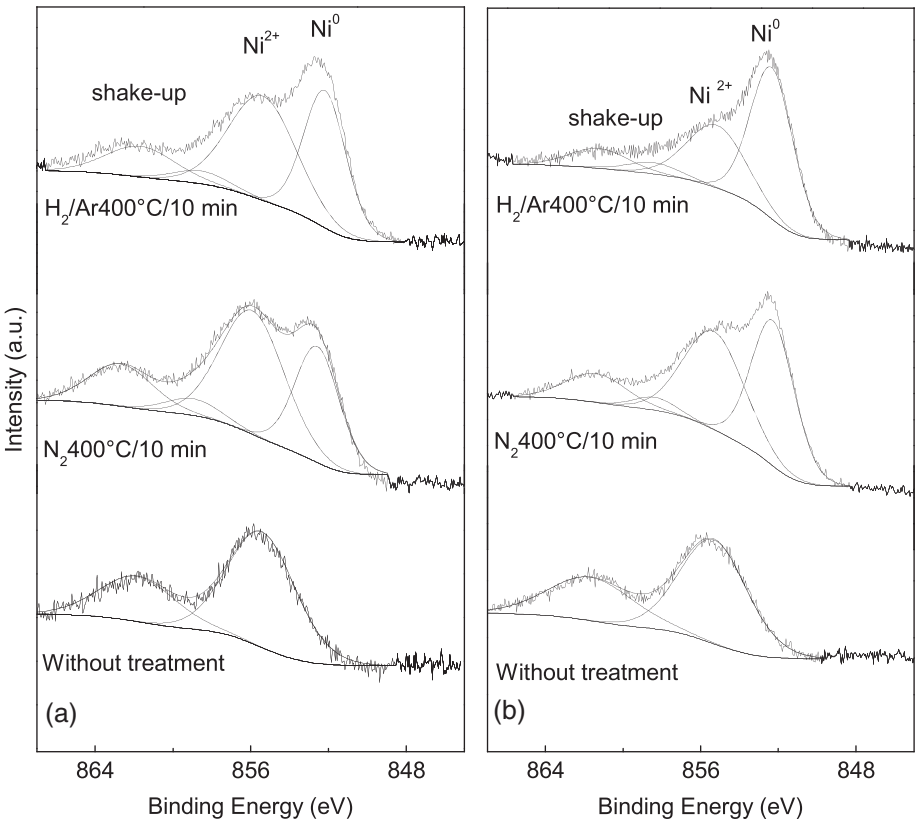

Figure 1. X-ray photoelectron spectra of (a) Ni(Nt)/MACe and (b) Ni(Nt)/MAPr in the Ni 2p region.

the Ni shake-up satellite, respectively. The BE values of Ni^{2+} are slightly higher than those assigned to NiO (854.4 eV) and close to those reported for Ni^{2+} in $NiAl_2O_4$.[17] This could be related to a strong metal–support interaction causing a shift to a higher BE. The presence of Ni^{2+} indicates that the surface oxidized species obtained by contact with the atmosphere (in agreement with TPR results) are not easily reduced at 400 °C in a H_2(5%)/Ar flow for 10 min.

In Table 2, the surface composition of Ni after the two treatments (in an inert and in a reductive atmosphere) and the Ni^0/Ni^{2+} surface ratios are shown. All samples presented a similar Ni surface concentration, between 0.07 and 0.08. Nevertheless, the Ni(Nt)/MAPr sample presented an Ni surface concentration of about twice as much that of the other samples (0.160 after treatment in N_2 atmosphere). In this sample, after 10 min of treatment in H_2(5%)/Ar flow at 400 °C, the Ni surface composition decreases 25%, suggesting a fast sintering of the metal. This fast sintering could explain the catalytic behavior of the Ni(Nt)/MAPr sample. This catalyst showed a complete ethanol conversion at the beginning of the reaction, a lower Ni particle size determined by XRD, a lower stability under reforming conditions and a significant amount of carbon formation (134%) (Table 3).[15] As it can be observed in

Table 2. XPS data of the catalyst after different treatments performed in the pre-treatment chamber of the spectrometer at 400 °C

Sample	*In situ* treatment	Ni/ (Ni+RE+Al+Mg)[a]	RE/(Ni+RE+Al+Mg)	Ni^0/Ni^{2+}	Ce^{3+}/Ce^{4+}
Ni(Nt)/MACe	N_2	0.074	0.036	0.60	0.30
	H_2/Ar	0.086	0.044	0.70	0.55
Ni(Ac)/MACe	N_2	0.070	0.030	0.74	0.54
	H_2/Ar	0.069	0.031	1.05	0.70
Ni(Nt)/MAPr	N_2	0.160	0.090	0.84	—
	H_2/Ar	0.120	0.080	1.30	—
Ni(Ac)/MAPr	N_2	0.080	0.060	1.10	—
	H_2/Ar	0.070	0.062	2.07	—
Ni(Nt)/MA	N_2	0.180	—	1.62	—
	H_2/Ar	0.170	—	1.73	—
MACe	N_2	—	0.031	—	0.19
	H_2/Ar	—	0.033	—	0.40

[a]RE: Ce or Pr.

Table 2, the Ni^0/Ni^{2+} ratio, as expected, increases after the H_2(5%)/Ar treatment during 10 min at 400 °C. For the catalysts promoted by Pr, a higher extent of reduction was observed compared with Ce-promoted ones. On the other hand, comparing the samples synthesized using different Ni precursors (nitrate or acetate), no significant difference on the Ni^0/Ni^{2+} surface ratio was observed.

The XPS spectra of the Ce 3d core level for the Ni(Nt)/MACe sample are shown in Fig. 2. The spectra were analyzed according to Larachi *et al.*[18] The complexity of the spectra in this region is due to the hybridization between partially occupied 4f orbital of Ce and the 2p levels of oxygen.[19–21] To perform the curve fitting of the spectra, restrictions on the BE positions and the fwhm were applied, according to Larachi *et al.*[18] A $3d_{5/2}:3d_{3/2}$ peak area ratio equal to 3 : 2 was constrained in the fitting procedure. In this region, features assigned to Ni $2p_{1/2}$ were also present. Figure 2b shows the peak assignments for Ce^{3+}, Ce^{4+} and Ni $2p_{1/2}$. Only the peaks related to Ce^{4+} were observed before any treatment in the lock-load chamber of the spectrometer (Fig. 2a). In this case, the spectrum was fitted by six peaks whose BEs were close to those assigned to CeO_2.[19] As reported in the literature,[18,21] the Ce 3d spectrum corresponding to CeO_2 is composed of several peaks; each component of the spin–orbit split 3d doublet contains three feature peaks referred to as *v*, *v*″, *v*‴ and *u*, *u*″, *u*‴ assigned to Ce $3d_{5/2}$ and Ce $3d_{3/2}$, respectively, (Fig. 2). Furthermore, the spectrum of Ce_2O_3 involves two peaks that are referred to as *v*°, *v*′ and *u*°, *u*′, to Ce $3d_{5/2}$ and Ce $3d_{3/2}$, respectively. Contrary to the sample without treatment, from the curve fitting of the spectra, peaks related to Ce^{3+} and Ce^{4+} could be observed after treatment of the solids in both inert and reductive atmospheres (Fig. 2a). The satellite peak associated with Ce $3d_{3/2}$ at about 916.5 eV is characteristic of the presence of Ce^{4+} on Ce compounds.[22] The pair positioned at about 885.5 and 904.0 eV are characteristic features of Ce_2O_3.[21] The main peak located at about 916.5 eV and the pair positioned at about 885.5 and 904.0 eV are characteristic features of CeO_2 and Ce_2O_3, respectively.[18]

The Ce^{3+}/Ce^{4+} ratio was estimated from curve fitting and integration of the Ce 3d region for each sample. The intensity ratio between the doublets assigned to Ce^{3+} and the total amount $[Ce^{3+} + Ce^{4+}]$ give the fraction of Ce^{3+}. Similar XPS data treatment was performed for all catalysts, and the results are included in Table 2. As it can be observed, the Ce^{3+}/Ce^{4+} ratio increases after reduction in about 80% for the Ni(Nt)/MACe and 30% for the Ni(Ac)/MACe catalyst in comparison with the ratio observed after treatment in N_2. Despite this, even after reduction in H_2(5%)/Ar flow up to 400 °C the couple Ce^{3+}/Ce^{4+} was observed in both samples. Comparing the catalytic performance of the solids, as mentioned earlier, both samples showed a good performance with a low conversion loss (Table 3). Nevertheless, it is important to note that the Ni(Nt)/MACe catalyst exhibited the lowest amount of carbonaceous deposits.

In contrast, for the Pr-promoted samples after both thermal treatments, only Pr^{3+} was observed by XPS (Fig. 3). The BEs at about 933 and 953 eV are assigned to the Pr $3d_{5/2}$ and Pr $3d_{3/2}$ peaks, respectively.[23] The shoulders observed at lower BEs are the shake-off satellite peaks.[21] A feature located at about

Table 3. Catalytic results in ethanol steam reforming[9]

Catalyst	Ethanol conversion[a] %	%XL[b]	Carbon amount %
Ni(Nt)/MACe	95.8	6.6	0.4
Ni(Ac)/MACe	97.1	2.2	24.1
Ni(Nt)/MAPr	68.7	31.1	134.2
Ni(Ac)/MAPr	89.2	14.7	1.0

[a]Final ethanol conversion after 600 min except to Ni(Nt)/MAPr, which is at 350 min.
[b]Conversion loss, $\%XL = \frac{X^0_{EtOH} - X^{SS}_{EtOH}}{X^0_{EtOH}} \times 100$.

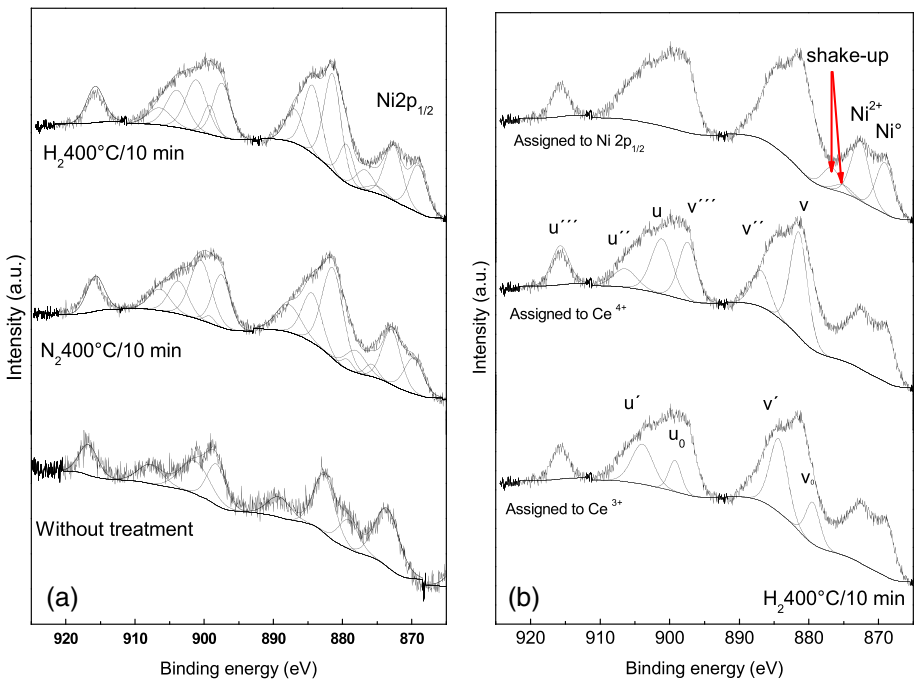

Figure 2. X-ray photoelectron spectra of Ni(Nt)/MACe catalyst in the Ce 3d region (a). Peak assignments for Ce^{3+}, Ce^{4+} and Ni $2p_{1/2}$ (b).

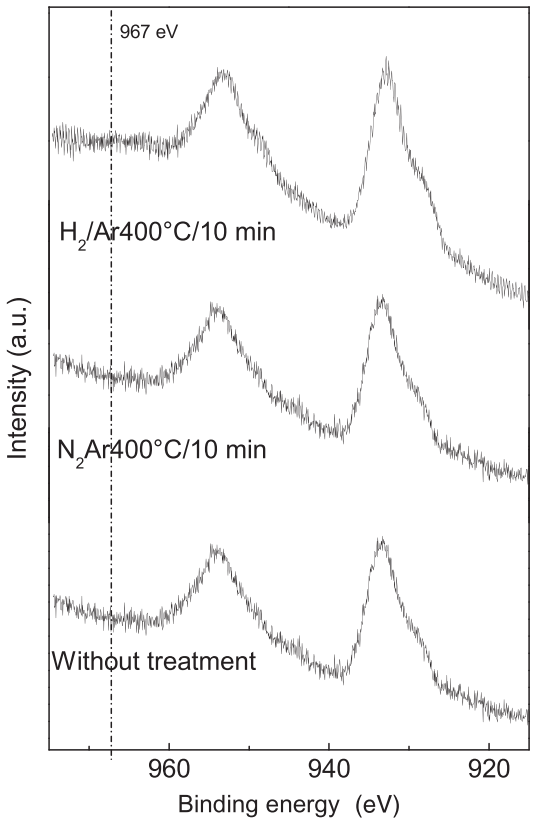

Figure 3. X-ray photoelectron spectra of Ni(Nt)/MAPr catalyst in the Pr 3d region.

968 eV due to the $3d4f^1$ final state is characteristic of tetravalent Pr and could be observed in both PrO_2 and Pr_6O_{11}.[24–26] In the Pr-promoted solids studied in this work, no feature located at ~967 eV could be observed (Fig. 3), which gives an indication that Pr is in a trivalent state at the surface.

The presence of the redox couple Ce^{3+}/Ce^{4+} at the surface of Ce-promoted catalysts could be related to the better performance of these catalysts, suggesting that it could be involved in the carbon deposition/removal mechanism. In the case of the Pr-containing solids, the redox mechanism associated with the carbon removal could be partially inhibited or slower.

It is worth noting that the Ni surface concentration decreases by the addition of the dopant as shown for the Ni(Nt)/MACe, Ni (Nt)/MAPr and Ni(Nt)/MA samples. In the literature, it has been reported that the addition of Ce increases Ni dispersion.[27,28] However, the surface atomic concentration for the catalyst presented in this work shows a decrease of about 60% for Ce-containing catalysts and 10% for Pr ones. Besides, the metallic dispersion for the Ce-containing catalysts increases or remains constant after reduction, whereas those with Pr decrease.

Particle size determination from XPS measurements

As it is known, different XPS models could be applied to determine the average particle size. In order to perform an estimation of the Ni^0 particle size after the treatments, the Davis model was applied.[16] This model is based on the intensity ratio between two peaks of the supported metal, coming from two different electronic levels that are sufficiently separated in energy. It is based on the diamond-shaped support particles and assumes that the electrons leave the sample with the emission angle of 45°. In comparison with other XPS models reported in the literature, such as Kerkhoff-Moulijn,[29] the main advantage of this model is the reduced dependence on the physical properties of the catalyst, such as support surface area and dispersed metal phase loading. The main requisite parameters for applying the model are the peak areas and the inelastic mean free path (IMFP, λ). The IMFPs used in this work were calculated with the Tougaard Quases-IMFP-TPP2M program.[30] The intensity ratio of two dispersed phase core levels is given as

$$\frac{I_1(d)}{I_2(d)} = \frac{\sigma_1 T_1 \lambda_1 \beta(d,\lambda_1)}{\sigma_2 T_2 \lambda_2 \beta(d,\lambda_2)} \quad (1)$$

where σ is the photoemission cross section, T is an instrumental transmission function that reflects the basic detection efficiency, λ is the IMFP of the primary photoelectron and β is the attenuation factor, which is characteristic of the particle shape and photoelectron attenuation length. This attenuation factor may be derived for different particle shapes using the relation given by Davis.[16] Assuming cubic dispersed phase morphology and that a not shadowing effect occurs, β is given by

$$\beta(d,\lambda) = 1 - \left(\frac{\lambda}{\sqrt{2}d}\right)\left[1 - \exp\left(-\frac{\sqrt{2}d}{\lambda}\right)\right]$$

where d is the particle size and could be obtained by iteration. More details about the calculations could be obtained from the original work.[16] This model was successfully applied by Wojcieszak *et al.* to determine Pd dispersion on Pd-supported nanoparticles.[31] In these solids, the presence of both states, Pd^0 and Pd^{2+}, was reported, and only the Pd^0 was taken into consideration in the model.

The two core levels studied for the Ni^0 particle size estimation were the Ni 2p with the BE at about 852 eV and the Ni 3p peak at about 65.7 eV, assigned to the Ni^0 species. The peak areas and BEs were obtained from curve fitting of the Ni 2p and Ni 3p spectrum by using the CasaXPS software. The Ni 3p spectrum was fitted by fixing the BE of the peaks assigned to Ni^0 and NiO, as well as the position of the corresponding satellites. Additionally, restrictions in the fwhm and main peak/satellite area ratio were applied considering the data reported in the literature.[32,33] As an example, Fig. 4 shows the Ni 3p spectra for the Ni(Nt)/MAPr catalyst after reduction in the treatment chamber of the spectrometer. Table 4 summarizes the Ni 3p/Ni 2p intensity ratio of the solids studied together with the corresponding ratio of the Ni reference sample. The particle sizes of the solids determined from the Davis model are also shown in Table 4. As it can be observed, the lowest Ni 3p/Ni 2p intensity ratio was obtained for the Ni(Nt)/MAPr catalyst, which exhibited the smaller particle size (about 5.8 nm). After reduction, the Ni^0 particle size of this solid increases up to 14 nm showing a fast sintering of the metal. In the same way, the Ni(Ac)/MAPr catalyst shows an increase in particle size from 21.5 to 34 nm, after reduction. For the solids with higher particle size, the Ni 3p/Ni 2p intensity ratio approached that for the Ni foil (0.21). In the Ce-promoted solids, the particle size remains practically constant after treatment in a reductive atmosphere (10 min H_2(5%)/Ar at 400 °C).The average particle sizes determined using the Davis model are also summarized in Fig. 5, and they are correlated with the normalized intensity ratio, which was calculated from the intensity ratio of the pure nickel sample and the studied solids. The minor discrepancies observed for larger particle sizes can

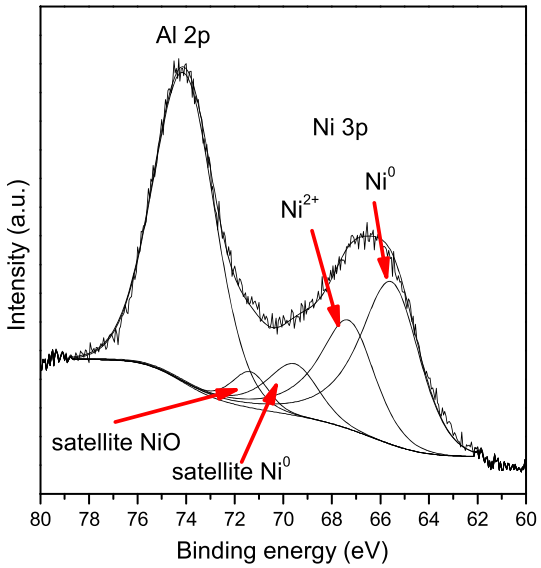

Figure 4. X-ray photoelectron spectra of Ni(Nt)/MAPr catalyst after reduction in the treatment chamber of the spectrometer in the Ni 3p region.

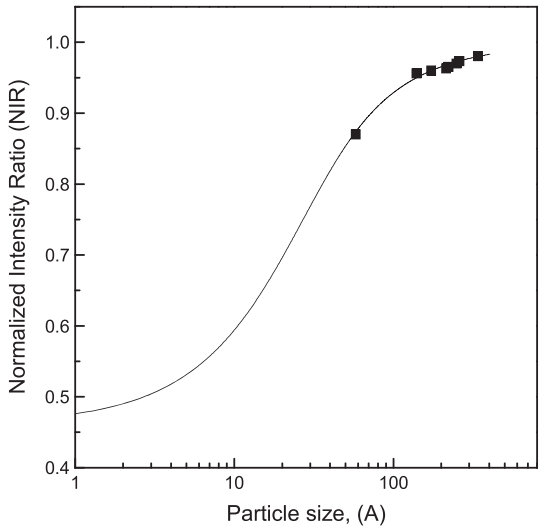

Figure 5. Ni^0 particle sizes calculated by the David model versus the normalized intensity ratio.

Table 4. Ni^0 particle size of the catalyst studied estimated by XPS and transmission electron microscopy

Sample	*In situ* treatment	Ni 3p/Ni 2p intensity ratio	[a]dp^{XPS} (nm)	[b]dp^{TEM} (nm)	[c]dp^{XRD} (nm)
Ni(Nt)/MACe	N_2	0.191	22.2	27.8	16.0
	H_2/Ar	0.185	17.3		
Ni(Ac)/MACe	N_2	0.206	26.0	27.6	28.0
	H_2/Ar	0.199	25.0		
Ni(Nt)/MAPr	N_2	0.163	5.8	15.7	5.0
	H_2/Ar	0.180	14.0		
Ni(Ac)/MAPr	N_2	0.190	21.5	20.8	42.0
	H_2/Ar	0.210	34.0		
Ni(Nt)/MA	N_2	0.185	17.3	—	—
	H_2/Ar	0.208	34.0		
Ni reference	—	0.210	—	—	—
MA	—	—	—	—	35.0

[a]Estimated using the Davis model, with the support particle size = 350 Å, λ_{3p}^{Ni} (1188) = 17.50 Å, λ_{2p}^{Ni} (401) = 8.14 Å, λ_{3p}^{Sop} (1188) = 23 Å, λ_{2p}^{Sop} (1188) = 10.5 Å.

[b]The particle size was determined from three micrographs of the fresh samples without treatments and was calculated as $d_s = \sum n_i d_i^3 / \sum n_i d_i^2$. A total of 150 particles were considered in the measurement.

[c]Calculations are based on (200) diffraction lines for Ni.[13]

be explained by the fact that the XPS intensity ratio becomes relatively insensitive to particle size changes for $d \geq 3\lambda$, in which case the prediction becomes strongly dependent upon the precision of the intensity ratio measurement. Another source of error that influences the particle size prediction is the presence of contaminant overlayers, being mainly evident with smaller particle sizes.[15] However, taking into account that the solids studied in this work were fresh samples and that they were heated up in the load-lock chamber of the spectrometer, we considered that no contamination error exists.

The TEM micrographs taken in the fresh samples and the particle size distribution are shown in Fig. 6. From the TEM pictures, high contrast and spherical particles were selected in agreement with the data reported in the literature.[32] The surface average size of the Ni^0 particles was calculated on the basis of size measurements of 150 particles for each catalyst in order to assure good statistic information. Three images were used because of the amount of particles available on each image. The average sizes of the dispersed particles determined by TEM are shown in Table 4, and they are compared with the data estimated from the Davis model and those determined by XRD.[9] As it can be observed, the Ni^0 particle sizes estimated from the Davis model are in good agreement with the TEM and XRD results, showing the same tendency between the solids. In Fig. 6, it can be seen that the Ce-doped solids exhibited a broader particle size distribution, with a low amount of particles with up to 50 nm. For the Ni(Nt)/MAPr sample, the particle size range was from 2.5 to 28 nm. It is important to note that the XRD and TEM measurements were performed on the fresh catalyst the particle size being comparable with the XPS data determined after treatment in N_2 flow. It should be noted that although some of the sizes of the Ni^0 particles are outside the range in which it is appropriate to apply the model, the data obtained from the XPS intensity ratio exhibited the same trends as those obtained by TEM and XRD. The smaller average particle size estimated was observed for the Ni(Nt)/MAPr sample, which showed an important sintering and a lower stability in ethanol steam reforming reaction. As reported by Davis,[16] the model is appropriate to estimate small particle size, between 1 and 5 nm.[16,25] Nevertheless, in the original work,[16] the author applied the model to estimate the particle size of oxidic and reduced Pd/Al_2O_3 catalysts. After calcinations at high temperature (600 °C), the particle size was larger than the range conveniently studied using the XPS intensity ratio approach. After hydrogen treatment of up to 500 °C, the Pd particle size increased up to about 13 nm, suggesting sintering of the dispersed phase or restructuring of the particle morphology. As a comparison, the particle sizes determined by TEM were also reported, showing that using the analysis of the dispersed phase XPS intensity ratio, an acceptable estimation of the particle size can be

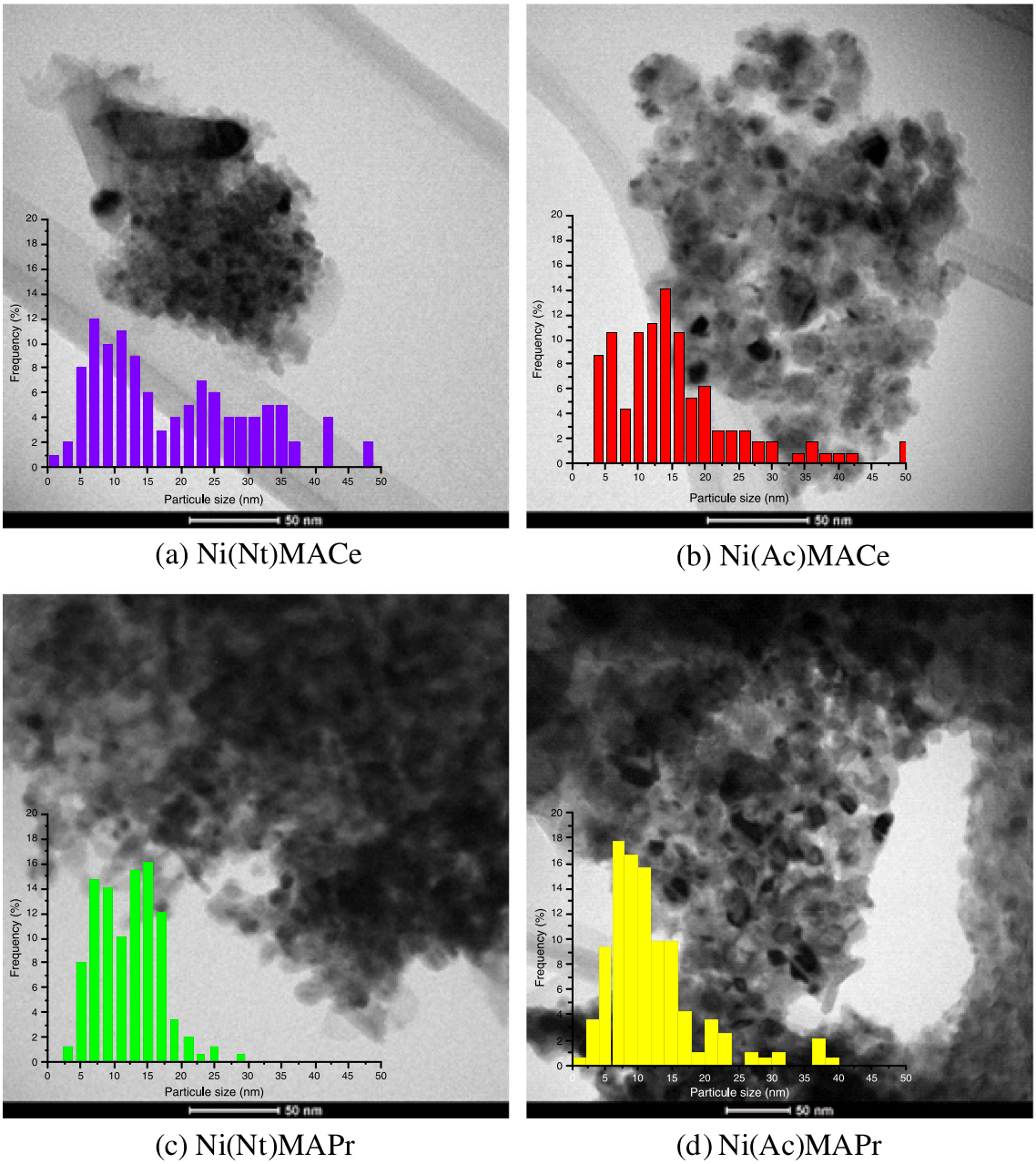

Figure 6. Transmission electron microscopy images and particle size distribution of the fresh catalysts: (a) Ni(Nt)/MACe, (b) Ni(Ac)/MACe, (c) Ni(Nt)/MAPr and (d) Ni(Ac)/MAPr.

achieved. For larger particle sizes, the prediction of the estimation became strongly dependent upon the accuracy of the intensity ratio measurement.[16] Additionally, for large particles, the size predictions became more influenced by changes in the intensity of the support layers. The David model has not been previously applied to the Ni^0 particle size determination. Therefore, the data reported in this work show a good correlation with the particle size determined by other techniques, indicating a potential application of the model to Ni-supported catalysts.

The clear increase in the particle size of the Pr-doped solids is probably due to a sintering effect under reductive atmosphere and could be related to the higher conversion loss of these catalysts, 14.7% and 31.1% for the Ni(Ac)/MAPr and Ni(Nt)/MAPr, respectively (Table 3). When the particle size of an Ni(Nt)/MA sample is compared with those obtained for the Ce-promoted and Pr-promoted solids (Table 4), it is possible to note that after reduction, smaller particles are obtained with the incorporation of Ce or Pr to the formulations. As stated earlier, it was reported that the addition of Ce increases the Ni dispersion of the catalyst.[27,29] The metallic dispersion for Ce-containing catalysts studied in this work increases or remains constant after reduction, whereas those with Pr decrease. Besides, note that between the Ce-doped solids, the Ni(Nt)/MACe exhibited the higher increase in the Ce^{3+}/Ce^{4+} ratio after reduction (about 80%) and the lower Ni^0 average particle size estimated by XPS and XRD (Table 4). These results provide evidence of the need for a model to estimate metal dispersion from XPS results.

Conclusions

In this work, the influence of reductive and inert treatments in the oxidation state of Ce or Pr as dopants of Ni catalysts was studied by XPS.

Ce-promoted catalysts presented no significant differences in the Ni surface concentration independent of both treatments. The promotion effect of Ce could be attributed to the Ce^{3+}/Ce^{4+} presence even at reductive atmosphere. Thus, the best performance in the ethanol steam reforming reaction over the Ni (Nt)/MACe catalyst could be associated with the high increase in the Ce^{3+}/Ce^{4+} surface ratio under reductive conditions.

Pr-doped catalysts showed a very high concentration of Pr^{3+} under a reductive atmosphere, and the redox behavior associated with the carbon removal could be partially inhibited or become slower. The Ni surface concentration on Ni(Nt)/MAPr decreased after the reduction treatment, suggesting a fast metallic sintering. This catalyst showed a high initial conversion in the ethanol steam reforming reaction, a high conversion loss and a considerable carbon amount.

By means of XPS data, the sintering of Ni^0 particles under reductive atmosphere was corroborated. The use of the Davis model allowed us to estimate the average size of Ni^0 particles, showing an increase after the treatment in H_2 for the Pr-promoted solids. The metal sintering under reductive atmosphere could be the reason for the higher loss of activity and carbon formation of the solids.

Acknowledgements

The authors wish to thank CONICET, ANPCyT, Universidad Nacional de San Luis and Universidad Nacional del Litoral for the financial support. The authors are grateful to ANPCyT for Grant PME 8-2003 to finance the purchase of the UHV Multi-Analysis System. Thanks are given to Prof. Elsa Grimaldi for the English language editing and to Dr. Antonio Monzón (University of Zaragoza, Spain) for assistance with TEM.

References

[1] A. M. da Silva, K. R. de Souza, G. Jacobs, U. M. Graham, B. H. Davis, L. V. Mattosa, F. B. Noronha, *Appl. Catal. B Env.* **2011**, *102*, 94–109.
[2] F. Wang, W. Cai, Tana, H. Provendier, Y. Schuurman, C. Descorme, C. Mirodatos, W. Shen, *Appl. Catal. B Env.* **2012**, *125*, 546–555.
[3] F. Frusteri, S. Freni, V. Chiodo, L. Spadaro, O. Di Blasi, G. Bonura, S. Cavallaro, *Appl. Catal. A Gen* **2004**, *270*, 1–7.
[4] L. V. Mattos, G. Jacobs, B. H. Davis, F. B. Noronha, *Chem. Rev.* **2012**, *112*, 4094–4123.
[5] D. Chen, K. O. Christensen, E. Ochoa-Fernández, Z. Yu, B. Totdal, N. Latorre, A. Monzón, A. Holmen, *J. Catal.* **2005**, *229*, 82–96.
[6] H. S. Bengaard, J. K. Nørskov, J. Sehested, B. S. Clausen, L. P. Nielsen, A. M. Molenbroek, J. R. Rostrup-Nielsen, *J. Catal.* **2002**, *209*, 365–384.
[7] A. Le Valant, N. Bion, F. Can, D. Duprez, F. Epron, *Appl. Catal. B Env.* **2010**, *97*, 72–81.
[8] A. Galetti, M. Gomez, L. Arrúa, M. C. Abello, *Appl. Catal. A Gen.* **2008**, *348*, 94–102.
[9] M. N. Barroso, A. Galetti, M. C. Abello, *Appl. Catal. A Gen.* **2011**, 394, 124–131.
[10] D. R. Mullins, *Surf. Sci.* **2004**, *556*, 159–170.
[11] V. Thangadurai, R. A. Huggins, W. Weppnar, *J. Solid State Electrochem.* **2001**, 5, 531–537.
[12] D. R. Mullins, K. Zhang, *J. Phys. Chem. B* **2001**, *105*, 1374–1380.
[13] Y. Borchert, P. Sonström, M. Wilhelm, H. Borchert, M. Bäumer. *J. Phys. Chem. C* **2008**, *112*, 3054–3063.
[14] G. Gallego, J. Marin, C. Batiot-Dupeyrat, J. Barrault, F. Mondragón, *Appl. Catal. A Gen.* **2009**, *369*, 97–103.
[15] A. E. Galetti, M. N. Barroso, M. F. Gómez, L. A. Arrúa, A. Monzón, M. C. Abello, *Catal. Lett.* **2012**, *142*, 1461–1469.
[16] S. M. Davis, *J. Catal.* **1989**, *117*, 432–446.
[17] H. Lei, Z. Song, X. Bao, X. Mu, B. Zong, E. Min, *Surf. Interface Anal.* **2001**, 32, 210–213.
[18] F. Larachi, J. Pierre, A. Adnot, A. Bernis, *Appl. Surf. Sci.* **2002**, *195*, 236–250.
[19] W. Xiao, Q. Guo, E. G. Wang, *Chem. Phys. Lett.* **2003**, *368*, 527–531.
[20] D. R. Mullins, S. H. Overbury, D. R. Huntley, *Surf. Sci.* **1998**, *409*, 307–319.
[21] P. Burroughs, A. Hamnet, A. F. Orchard, G. Thornton, *J. Chem Soc. Dalton* **1976**, 1686–1698.
[22] E. Bêche, P. Charvin, D. Perarnau, S. Abanades, G. Flamant, *Surf. Interface Anal.* **2008**, 40, 264–267.
[23] I. Tankov, B. Pawelec, K. Arishtirova, S. Damyanova, *Appl. Surf. Sci.* **2011**, *258*, 278–284.
[24] Z. Song, W. Liu, H. Nishiguchi, A. Takami, K. Nagaoka, Y. Takita, *Appl. Catal. A Gen.* **2007**, *329*, 86–92.
[25] H. Borchert, Y. Frolova, V. Kaichev, I. Prosvirin, G. M. Alikina, A. Lukashevich, V. Zaikovskii, E. Moroz, S. Trukhan, V. Ivanov, E. Paukshtis, V. Bukhtiyarov, V. A. Sadykov, *J. Phys. Chem. B* **2005**, *109*, 5728–5738.
[26] S. Lutkehoff', M. Neumann, A. Slebarski, *Phys. Rev. B* **1995**, *52*, 808–811.
[27] S. Wang, G. Q. Lu, *Appl. Catal. B Env.* **1998**, 19, 267–277.
[28] K. Y. Koo, H.-S. Roh, U. H. Jung, W. L. Yoon, *Catal. Lett.* **2009**, *130*, 217–221.
[29] A. Cimino, D. Gazzoli, M. Valigi, J. Electron, *Spec. Rel. Phen.* **1999**, *104*, 1–29.
[30] S. Tougaard, QUASES-IMPF-TPP2M program; Quases-Tougaard Inc.
[31] R. Wojcieszak, M. J. Genet, P. Eloy, P. Ruiz, E. M. Gaigneaux, *J. Phys. Chem. C* **2010**, *114*, 16677–16684.
[32] A. N. Mansour, *Surf. Sci. Spectra* **1994**, 3, 231–238.
[33] S. Hüfner, G. K. Wertheim, *Phys. Lett.* **1975**, *51A*, 301–303.

